PAPER • OPEN ACCESS

Energy deposition and deflection of α particles in hot dense plasmas relevant to inertial confinement fusions

To cite this article: Chengliang Lin *et al* 2023 *Nucl. Fusion* **63** 076018

OPEN ACCESS
IOP Publishing | International Atomic Energy Agency
Nuclear Fusion
Nucl. Fusion **63** (2023) 076018 (13pp)
https://doi.org/10.1088/1741-4326/acd19f

Energy deposition and deflection of α particles in hot dense plasmas relevant to inertial confinement fusions

Chengliang Lin[1], Bin He[1,*], Yong Wu[1,2,*] and Jianguo Wang[1]

[1] National Key Laboratory of Computational Physics, Institute of Applied Physics and Computational Mathematics, Beijing, China
[2] Center for Applied Physics and Technology, HEDPS, Peking University, Beijing, China

E-mail: hebin-rc@163.com and wu_yong@iapcm.ac.cn

Received 5 September 2022, revised 17 March 2023
Accepted for publication 2 May 2023
Published 31 May 2023

Abstract

Based on the kinetic theory, improved T-matrix models for the continuous-slowing-down and the linear-energy-transfer stopping powers are established at the same level, where multiple scattering effects and the related transverse deflection are accounted for consistently and systematically. The degree of deflection characterizing the extent of transverse deflection is defined by means of the ratio of these two stopping powers. Calculations for the energy deposition and deflection of α particles in hot dense deuterium–tritium (DT) plasmas and also in hot dense DT plasmas mixed with carbon (C) impurities are performed. Multiple scattering effects and the resulting transverse deflection are demonstrated to have a significant influence on the stopping power of α particles, in particular, in mixtures containing different ions with large mass and charge asymmetry. It is shown that for DT plasma mixed with 5% C impurities, the range and penetration depth of the α particle are shortened by about 21% and 27%, respectively. Our models are found to be appropriate for the evaluation of stopping powers not only in weakly coupled plasmas but also in moderately degenerate and correlated plasmas. These results manifest that multiple scattering effects and the induced transverse deflection need to be taken into account in modeling the transport of α particles in hot dense plasmas relevant to inertial confinement fusion.

Keywords: stopping power, deflection of α particles, deuterium–tritium plasmas, inertial confinement fusion, quantum kinetic theory, energy deposition

(Some figures may appear in colour only in the online journal)

* Authors to whom any correspondence should be addressed.

1. Introduction

The knowledge of stopping power or energy loss of energetic charged particles (denoted as test particles) in dense systems is of fundamental importance across a wide range of disciplines, such as condensed matter physics [1] and plasma physics [2, 3]. In the case of plasmas, an accurate treatment of the stopping power is crucial for most inertial fusion applications [3], such as for understanding the self-heating mechanism and for predicting the ignition condition and fusion energy gain, as well as for the design of the ignition targets. For the modeling of self-heating in deuterium–tritium (DT) fusion, precisely calculating the stopping power of α particles initially at the birth energy of 3.54 MeV is a prerequisite for studying the energy balance and dynamical evolution in the hot spot of fusion fuel [3, 4].

In modeling the transport of α particles in inertial confinement fusion (ICF) systems, the α particle is usually assumed to move along a straight line, and its transverse deflection (or diffusion) is assumed to be insignificant. The reason for assuming rectilinear motion is that the energy of α particles is mainly deposited on the plasma electrons [2, 5, 6], which gives rise to negligible sideways motion. However, transverse deflection can play a critical role in ICF plasmas, especially toward the end of the range of α particles, because large-angle scattering of collisions between α particles and plasma ions can result in strong transverse diffusion of the α particle with respect to their initial direction of motion. As will be demonstrated in the current work, the transverse deflection has a significant influence on the stopping power and energy deposition of α particles in DT plasma, in particular when heavy and highly charged impurities exist. In fact, ionic mixtures are ubiquitous in ICF systems. For example, high-Z materials (e.g. gold used as a high-Z pusher) exist in the inner shell of double-shell targets for the volume ignition scheme [3, 7, 8], where fusion product deflection induced by collisions with high-Z ions could be important. Moreover, in the hot-spot ignition scheme, the DT fuel layer is enclosed by an ablator shell (such as beryllium, copper-doped beryllium, silicon-doped plastic or high-density carbon) [9, 10], where the ablator material can mix into the DT hot spot [11–13]. Such mixing can significantly affect the transport and energy deposition of α particles in the hot spot. Therefore, an accurate microscopic description of large-angle scattering and multiple scattering effects on the stopping powers and deflections of fusion products is urgently demanded.

The problem of deflection has been extensively investigated for the stopping of energetic electrons produced in the fast ignition of thermonuclear fusion [14, 15], where the Boltzmann equation in the diffusion approximation is utilized to describe the effects of multiple scattering [16, 17]. The utilization of diffusion approximation in the Boltzmann equation indicates that the plasma particles are assumed to be stationary, which implicitly corresponds to assuming that the target is cold and that the target particles are much heavier than the incident test particle. However, these assumptions are not appropriate for hot plasma systems under conditions relevant to inertial fusion. Firstly, the temperature of ICF plasmas is usually very high, so the velocity distribution of plasma particles has to be taken into account. Secondly, the masses of the fusion products and the plasma ions are comparable, such as $m_\alpha/m_{\rm DT} \approx 1.6$ for DT fusion. Although a modification of the multiple scattering theory for the degree of deflection has been proposed [18], the aforementioned assumptions are not removed completely. A more systematic and accurate theory is required to describe the inherent relation between the transverse deflection and the stopping power of the test particle.

To determine the degree of transverse deflection, a detailed knowledge of the stopping power is a fundamental ingredient. In general, two different definitions of stopping power exist in the literature [2, 19–22], namely the continuous-slowing-down (CSD) and linear-energy-transfer (LET) stopping power. The CSD stopping power $\mathrm{d}E/\mathrm{d}s$ describes the transfer rate of kinetic energy of the charged particle in plasmas [2, 20], while the LET stopping power $\mathrm{d}E/\mathrm{d}x$ is determined by the decelerating force that measures the change in test particle momentum projected in the direction of initial motion [2, 21, 22]. The distinction between these two stopping powers characterizes the transverse deflection of a test particle with respect to its incident direction [5, 14, 23]. Once the CSD and LET stopping powers can be determined at the same level, a consistent picture for the transport and energy loss of test particles in dense plasmas can be achieved.

In the present work, we present a systematic and self-consistent approach to determine the degree of deflection through the CSD and LET stopping powers. For this purpose, improved T-matrix (ITM) models are developed to calculate both the CSD and LET stopping power on the same footing. This paper is organized as follows: in section 2.1, the definition of the degree of deflection is discussed. Following a kinetic approach within the quantum statistical framework [2, 24], detailed descriptions for the CSD and LET stopping power are elucidated in section 2.2. Subsequently, quantum theory for the transport cross-section is briefly reviewed in section 2.3, where a velocity-dependent screening length is introduced to account for dynamic effects in dense plasmas. In section 3.1, we present the results of energy deposition and deflection of α particles in DT plasmas. Similar investigations in DT+C mixtures are carried out in section 3.2. Conclusions are drawn in section 4. Additionally, derivations for the CSD and LET stopping power as well as the transverse deflection of test particles are described in detail in the appendix.

2. Methodology

2.1. Statement of the problem for degree of deflection and stopping powers

For the modeling of stopping powers, the elementary quantity is the change in test particle momentum due to scattering effects. The multiple scattering effect caused by the large number of small- and large-angle collisions not only results

in deceleration along the incident direction, but also leads to transverse diffusion of the test particle perpendicular to the initial incident direction [23]. Hence, it is more convenient to decompose the test particle momentum into longitudinal and transverse components with respect to the direction of original motion, i.e. $\mathbf{p}_\mathrm{T} = \mathbf{p}_\mathrm{T}^{\perp} + \mathbf{p}_\mathrm{T}^{\parallel}$. This decomposition leads to the relation $\mathbf{p}_\mathrm{T}^2 = (\mathbf{p}_\mathrm{T}^{\perp})^2 + (\mathbf{p}_\mathrm{T}^{\parallel})^2$, which also holds for their time derivatives. Averaging over the plasma ensemble yields the following expression for the test particle [23]:

$$\frac{\mathrm{d}}{\mathrm{d}t}\left\langle \frac{\mathbf{p}_\mathrm{T}^2}{2m_\mathrm{T}} \right\rangle = \frac{\mathbf{p}_\mathrm{T}}{m_\mathrm{T}} \cdot \frac{\mathrm{d}}{\mathrm{d}t}\langle \mathbf{p}_\mathrm{T} \rangle + \frac{\mathrm{d}}{\mathrm{d}t}\left\langle \frac{(\mathbf{p}_\mathrm{T}^{\perp})^2}{2m_\mathrm{T}} \right\rangle . \tag{1}$$

In the language of stopping powers, the term on the left-hand side of equation (1) is directly connected to the CSD stopping power $\mathrm{d}E/\mathrm{d}s$, and the first term on the right-hand side describes the LET stopping power $\mathrm{d}E/\mathrm{d}x$ [2, 22]. The last term in equation (1) manifests the transverse motion of the test particle under the influence of collisions, and determines the degree of deflection. Therefore, the decomposition of momentum provides an unambiguous physical picture for different stopping powers. Because the stopping powers $\mathrm{d}E/\mathrm{d}s$ and $\mathrm{d}E/\mathrm{d}x$ are negatively defined with respect to the incident energy of the test particle, the LET stopping power $\mathrm{d}E/\mathrm{d}x$ defines the hypotenuse of the right triangle, whereas the CSD stopping power $\mathrm{d}E/\mathrm{d}s$ and the energy change related to $(\mathbf{p}_\mathrm{T}^{\perp})^2$ are associated with the legs of the right triangle. Consequently, the degree of deflection resulting from the multiple scattering effects is defined by the CSD and LET stopping powers of the test particle [14]:

$$\langle \cos\theta \rangle = \frac{\mathrm{d}E}{\mathrm{d}s}\left(\frac{\mathrm{d}E}{\mathrm{d}x}\right)^{-1} . \tag{2}$$

This definition is widely utilized to describe the mean deflection of directed energetic electrons in plasmas [14, 15]. The degree of deflection $\langle \cos\theta \rangle$ (2) is a basic element in Monte Carlo code for the simulation of dynamical evolution of ICF systems [15, 25, 26]. Note that, unlike the notation used in [14], the notation of the mean deflection angle in the present work is referred to $\theta = \arccos\langle \cos\theta \rangle$, whereas the degree of deflection is named for the quantity $\langle \cos\theta \rangle$.

In the framework of multiple scattering theory for the degree of deflection $\langle \cos\theta \rangle$ [14, 15, 18], the CSD stopping power $\mathrm{d}E/\mathrm{d}s$ is first evaluated using well-known approaches such as the Brown, Preston and Singleton (BPS) [5] or Li and Petrasso (LP) model [27–29], with which $\langle \cos\theta \rangle$ is then calculated according to $\langle \cos\theta \rangle = \exp\left\{ -\int_{E_0}^{E} \mathrm{d}E\, k_\mathrm{mfp}(E) \left(\frac{\mathrm{d}E}{\mathrm{d}s}\right)^{-1} \right\}$, with $k_\mathrm{mfp}(E)$ being the total inverse mean free path induced by collisions with plasma particles [15]. Then, the LET stopping power $\mathrm{d}E/\mathrm{d}x$ is determined from the relation (2). This procedure is only suitable for the description of stopping and deflection of energetic electrons in dense plasmas. For energetic ions transiting hot dense systems, such a description based on diffusion approximation breaks down. In fact, direct calculation of the degree of deflection $\langle \cos\theta \rangle$ in dense multicomponent plasmas can be accomplished using the relation (2), once accurate approaches for both the $\mathrm{d}E/\mathrm{d}s$ and $\mathrm{d}E/\mathrm{d}x$ stopping powers have been developed at the same level.

For practical purposes, different authors have paid attention to one of these two stopping powers. The BPS and LP models are well developed for calculating $\mathrm{d}E/\mathrm{d}s$, while the density functional formalism for stopping power can be applied to excellently simulate $\mathrm{d}E/\mathrm{d}x$ [30, 31]. The dielectric formalism can be applied to calculate the CSD and LET stopping powers in weakly coupled plasmas [2]. Usually, the energy loss of ions is assumed to be dominated by free electrons. The transverse deflection induced by ion–electron collisions is generally a small effect of relative order $m_\mathrm{e}/m_\mathrm{T}$ with respect to the longitudinal motion [5], so that the difference between the CSD and LET stopping power is negligible. This is the reason why only one of these two stopping powers is required to explain the experimental measurements and numerical simulations. However, plasma ions contribute significantly to the energy loss of test particles, especially in the low-velocity region, where the transverse spreading of the test projectile also becomes non-negligible. Therefore, advanced approaches for the calculation of stopping powers and transverse deflection are necessary. In the subsequent subsection, consistent and systematic ITM models for the CSD and LET stopping power and the related transverse diffusion are proposed based on the kinetic theory [2].

2.2. *Kinetic approaches for energy loss and stopping power in plasmas*

According to the kinetic theory [2, 24], the transfer rate of a certain relevant physical quantity $\mathcal{A} = \mathcal{A}(\mathbf{p}_\mathrm{T})$ induced by the interaction of test particles with plasma particles is represented by

$$\frac{\mathrm{d}}{\mathrm{d}t}\langle \mathcal{A} \rangle = \frac{1}{n_\mathrm{T}} \int \frac{d^3\mathbf{p}_\mathrm{T}}{(2\pi\hbar)^3}\, \mathcal{A}(\mathbf{p}_\mathrm{T})\, \frac{\mathrm{d}}{\mathrm{d}t} f_\mathrm{T}(\mathbf{p}_\mathrm{T}, t) , \tag{3}$$

where n_T is the number density of the test particle, and the test particle momentum $\mathbf{p}_\mathrm{T} = m_\mathrm{T}\mathbf{v}_\mathrm{T}$ is defined by the product of mass m_T and velocity $\mathbf{v}_\mathrm{T}$ of the test particle. Here $f_\mathrm{T}(\mathbf{p}_\mathrm{T}, t)$ denotes the test particle distribution function and $\mathrm{d}f_\mathrm{T}/\mathrm{d}t$ represents the collision integral (for details see appendix). From the formalism (3) with special choice for the quantity $\mathcal{A}(\mathbf{p}_\mathrm{T})$, expressions for the CSD and LET stopping power can be derived. Derivation of the results of the stopping powers $\mathrm{d}E/\mathrm{d}s$ and $\mathrm{d}E/\mathrm{d}x$ are presented in the appendix. In this subsection, only the central expressions are summarized.

For the LET stopping power $\mathrm{d}E/\mathrm{d}x$, the relevant quantity $\mathcal{A}(\mathbf{p}_\mathrm{T})$ is the test particle momentum [2, 22]. The LET stopping power $\mathrm{d}E/\mathrm{d}x$ is related to the change of momentum along the initial incident direction before and after the collision $\mathcal{A}_\mathrm{M}(\mathbf{p}_\mathrm{T}') - \mathcal{A}_\mathrm{M}(\mathbf{p}_\mathrm{T}) = \mathbf{v}_\mathrm{T} \cdot (\mathbf{p}_\mathrm{T}' - \mathbf{p}_\mathrm{T})$, which is determined through the momentum transfer rate

$$\frac{\mathrm{d}E}{\mathrm{d}x} = \frac{1}{v_\mathrm{T}} \frac{\mathrm{d}}{\mathrm{d}t} \langle \mathcal{A}_\mathrm{M} \rangle . \tag{4}$$

After straightforward algebra, we obtain the following representation for the LET stopping power:

$$\frac{\mathrm{d}E}{\mathrm{d}x} = \sum_c \mathcal{U}_{\mathrm{T}c} \frac{m_c}{\sqrt{\pi}\mu_{\mathrm{T}c}} \int_0^\infty \frac{\mathrm{d}z}{z^2} \mathcal{L}_{\mathrm{T}c}(u,z)\, \widetilde{\mathcal{F}}_{\mathrm{M}}(u,z), \tag{5}$$

with $\mathcal{U}_{\mathrm{T}c} = z_{\mathrm{T}}^2 \mathrm{e}^2 \omega_{\mathrm{pl},c}^2 / \left(4\pi\epsilon_0 v_{\mathrm{T}}^2\right)$ characterizing the unit of stopping power and the function

$$\widetilde{\mathcal{F}}_{\mathrm{M}}(u,z) = \mathrm{e}^{-\left(u^2+z^2\right)} \left[\sinh(2uz) - 2uz\cosh(2uz)\right]. \tag{6}$$

Here, $\mu_{\mathrm{T}c} = m_{\mathrm{T}} m_c/(m_{\mathrm{T}}+m_c)$ and $z = v_{\mathrm{T}c}/v_{\mathrm{th},c}$ are the reduced mass and the reduced relative velocity of the scattering pair, respectively. $u = v_{\mathrm{T}}/v_{\mathrm{th},c}$ denotes the reduced velocity of the test particle. The parameters $\omega_c^2 = z_c^2 \mathrm{e}^2 n_c/(\epsilon_0 m_c)$ and $v_{\mathrm{th},c}^2 = 2k_{\mathrm{B}}T_c/m_c$ represent the plasma frequency and thermal velocity of plasma particle species c. The velocity-dependent Coulomb logarithm $\mathcal{L}_{\mathrm{T}c}(u,z)$ is defined through the transport cross-section $\mathcal{Q}_{\mathrm{T}c}(v_{\mathrm{T}},p)$ [32]:

$$\mathcal{L}_{\mathrm{T}c}(u,z) = \frac{\mathcal{Q}_{\mathrm{T}c}(v_{\mathrm{T}},p)}{4\pi\, b_{\mathrm{T}c}^2} \tag{7}$$

with $b_{\mathrm{T}c} = z_{\mathrm{T}} z_c e^2/(4\pi\epsilon_0\mu_{\mathrm{T}c}v_{\mathrm{T}c}^2)$ denoting the classical impact parameter for 90° deflection subjected to pure Coulomb interaction.

The relevant quantity $\mathcal{A}(\mathbf{p}_{\mathrm{T}})$ to calculate the CSD stopping power $\frac{\mathrm{d}E}{\mathrm{d}s} = \frac{1}{v_{\mathrm{T}}}\frac{\mathrm{d}}{\mathrm{d}t}\langle\mathcal{A}_{\mathrm{E}}\rangle$ is the kinetic energy of the test particle with its change before and after collision given by $\mathcal{A}_{\mathrm{E}}(\mathbf{p}_{\mathrm{T}}') - \mathcal{A}_{\mathrm{E}}(\mathbf{p}_{\mathrm{T}}) = (\mathbf{p}_{\mathrm{T}}'^2 - \mathbf{p}_{\mathrm{T}}^2)/(2m_{\mathrm{T}})$ [2, 22]. The resulting formula for the CSD stopping power is

$$\frac{\mathrm{d}E}{\mathrm{d}s} = \sum_c \mathcal{U}_{\mathrm{T}c} \frac{m_c}{\sqrt{\pi}\mu_{\mathrm{T}c}} \int_0^\infty \frac{\mathrm{d}z}{z^2} \mathcal{L}_{\mathrm{T}c}(u,z)\, \widetilde{\mathcal{F}}_{\mathrm{E}}(u,z) \tag{8}$$

with the function $\widetilde{\mathcal{F}}_{\mathrm{E}}(u,z)$ given by

$$\widetilde{\mathcal{F}}_{\mathrm{E}}(u,z) = \left[\left(1+2z^2\frac{\mu_{\mathrm{T}c}}{m_{\mathrm{T}}}\right)\sinh(2uz) - 2uz\cosh(2uz)\right] \cdot \times \exp\left[-\left(u^2+z^2\right)\right]. \tag{9}$$

Similarly, the transverse diffusion is described by the following expression:

$$\mathcal{D}_\perp = \sum_c \mathcal{U}_{\mathrm{T}c} \frac{2m_c}{\sqrt{\pi}m_{\mathrm{T}}} \int_0^\infty \mathrm{d}z\, \mathcal{L}_{\mathrm{T}c}(u,z)\, \widetilde{\mathcal{F}}_\perp(u,z), \tag{10}$$

where the function $\widetilde{\mathcal{F}}_\perp(u,z)$ reads

$$\widetilde{\mathcal{F}}_\perp(u,z) = \mathrm{e}^{-\left(u^2+z^2\right)} \sinh(2uz). \tag{11}$$

Expressions similar to equations (5) and (8) are also presented in [2, 20, 21]. Recently, models for the CSD and LET stopping powers were also proposed with the use of an effective potential theory for the collision integral [33]. From expression (1), it can be concluded that the multiple scattering effects are only partly considered in the CSD stopping power $\mathrm{d}E/\mathrm{d}s$ and fully included in the LET stopping power $\mathrm{d}E/\mathrm{d}x$ in the frame of binary collision description. Obviously, the missing part of the multiple scattering effects in $\mathrm{d}E/\mathrm{d}s$ is connected to the transverse deflection $\mathcal{D}_\perp$ (10) and is characterized by the degree of deflection $\langle\cos\theta\rangle$ (2).

To derive the stopping powers (5) and (8) as well as the transverse deflection (10), the on-shell T-matrix approximation is implemented. In this approximation, the full many-body effects within the binary collision approximation are reasonably accounted for through a statically screened potential determined from the self-energy in terms of ladder summation [2, 24]. Hence, the effects of strong collisions and multiple scattering are satisfactorily taken into account. However, dynamical screening effects and plasmon excitations are completely neglected in the on-shell T-matrix approximation. Therefore, more elaborate approaches are needed to incorporate binary collision contributions from the strong coupling region and dynamical effects. In the realm of kinetic theory, the most commonly used approach is a combined scheme using both a static T-matrix description and a dynamical dielectric response [21, 24], which was originally introduced by Gould and DeWitt for the calculation of transport properties in plasmas [34]. In this approach, the dynamical effects are included by introducing the linear response cross-section through the dielectric function. In the present work, another theoretical scheme proposed in [35] is utilized, where effects induced by dynamically screened interaction are mapped into the T-matrix description with the use of a spherically symmetric velocity-dependent interaction potential. We will discuss this scheme in detail in the subsequent subsection.

2.3. *Transport cross-sections and velocity-dependent screening length*

The central quantity for the determination of stopping powers $\mathrm{d}E/\mathrm{d}x$ (5), $\mathrm{d}E/\mathrm{d}s$ (8) and transverse deflection $\mathcal{D}_\perp$ (10) as well as the degree of deflection $\langle\cos\theta\rangle$ (2) is the velocity-dependent Coulomb logarithm $\mathcal{L}_{\mathrm{T}c}(u,z)$. This is related to the transport cross-section $\mathcal{Q}_{\mathrm{T}c}(p)$. In accordance with the quantum collision theory, the transport cross-section can be evaluated through the partial wave analysis [36]

$$\mathcal{Q}_{\mathrm{T}c}^{\mathrm{qm}}(v_{\mathrm{T}},p) = \frac{4\pi}{p^2}\sum_{l=0}^{\infty}(l+1)\sin^2\left[\delta_l(p) - \delta_{l+1}(p)\right]. \tag{12}$$

The phase shifts $\delta_l(p)$ acquired from the solution of the radial Schrödinger equation depend on the test particle velocity due to the employment of the velocity-dependent potential. For high-temperature plasmas, scattering phase shifts at large partial waves and high energies are generally required to calculate the transport cross-sections (12). To alleviate the computational cost, it is desirable to incorporate the Born and WKB phase shifts into the calculation of transport cross-sections. For this purpose, quantitative criteria for the applicability of Born and WKB approximations need to be established. Such a procedure was proposed by the authors in [37], and was applied in this work to calculate

$\mathcal{Q}^{\rm qm}_{{\rm T}c}(v_{\rm T},p)$ of projectile-electron scattering. For collisions between ionic projectile and plasma ions, quantum mechanical treatment (12) is generally unnecessary and the classic transport cross-section can be applied [38]:

$$\mathcal{Q}^{\rm cl}_{{\rm T}c}(v_{\rm T},p)=2\pi\int_0^\infty {\rm d}b\, b\,(1-\cos\chi) \tag{13}$$

where b is the impact parameter and χ is the scattering angle given by

$$\chi=\pi-2b\int_{r_0}^\infty \frac{{\rm d}r}{r^2}\left[1-\frac{b^2}{r^2}-\frac{2\mu_{{\rm T}c}}{p^2}V^{\rm S}_{{\rm T}c}(v_{\rm T},r)\right]^{-1/2} \tag{14}$$

with the outermost classical turning point r_0. In the present study, the quantum mechanical transport cross-section (12) is utilized in the Coulomb logarithm (7) for electron–ion collisions, whereas the classic transport cross-section (13) is applied for ion–ion scattering.

For the purpose of calculating $\mathcal{Q}_{{\rm T}c}$, the velocity-dependent Yukawa potential is employed here, through which dynamical effects and collective excitations are included in the average sense [22, 35, 39]:

$$V^{\rm S}_{{\rm T}c}(v_{\rm T},r)=\frac{z_{\rm T}z_c e^2}{4\pi\epsilon_0 r}\exp\left[-\frac{r}{\lambda_{\rm s}(v_{\rm T})}\right]. \tag{15}$$

This potential is demonstrated to be appropriate to calculate the stopping power of charged particles in weakly and moderately coupled plasmas [40, 41]. The choice of an appropriate screening length $\lambda_{\rm s}(v_{\rm T})$ is crucial for imitating the dynamical effects at medium velocities [22]. Generally, the following form is widely used to effectively describe the dynamical screening effects and collective excitations in the stopping power calculation [22, 39, 40, 42]:

$$\lambda^0_{\rm s}(v_{\rm T})=\frac{1}{\kappa_{\rm s}}\sqrt{1+x^2_{\rm T}}. \tag{16}$$

where $x_{\rm T}=v_{\rm T}\kappa_{\rm s}/\omega_{\rm pl,e}$ with the screening parameter $\kappa^2_{\rm s}=\frac{{\rm e}^2 n_{\rm e}}{2\epsilon_0 k_{\rm B}T_{\rm e}}\frac{F_{-1/2}(\eta_{\rm e})}{F_{1/2}(\eta_{\rm e})}$ defined in terms of the Fermi integral $F_a(y)=\int_0^\infty {\rm d}x x^a/[\exp(x-y)+1]$ [2]. In the low-velocity limit $v_{\rm T}\to 0$, the static Debye-like potential is recovered from equation (16). For a swift test particle that moves with velocities much larger than $\omega_{\rm pl,e}/\kappa_{\rm s}$, the effective interaction range is determined by Bohr's adiabatic radius $v_{\rm T}/\omega_{\rm pl,e}$ [39, 42].

Although dynamical effects can be treated in a satisfactory manner with simple interpolation (16), it is inadequate to capture some critical features for the stopping power calculation. In particular, using the screening length (16) to study the stopping number, an additional term $-1/2$ will appear for high velocities compared to Bethe's stopping formula [42]. This problem is directly related to the high velocity asymptotic behavior of the screening length $\lambda_{\rm s}(v_{\rm T})$. As discussed in [35], mapping the dynamical effects contained in the linear response description into the pure T-matrix description leads to an asymptotic behavior in the high-velocity limit characterized by $\kappa_{\rm s}\lambda_{\rm s}(v_{\rm T})\sim {\rm e}^{1/2}x_{\rm T}$. In the present work, the following interpolation is proposed for the screening length:

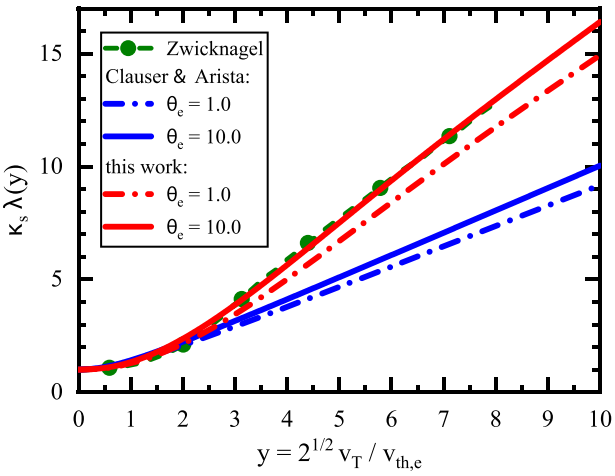

Figure 1. Velocity-dependent screening length $\kappa_{\rm s}\lambda_{\rm s}(v_{\rm T})$ as a function of $\sqrt{2}v_{\rm T}/v_{\rm th,e}$. The green dashed lines with circles denote the numerical results for non-degenerate electron gas reported by Zwicknagel [35]. The blue lines represent the calculations using the model (16). The red lines give the results calculated from (17) for different degeneracy parameters.

$$\lambda_{\rm s}(v_{\rm T})=\frac{1}{\kappa_{\rm s}}\sqrt{1+\frac{\rm e}{2}\left\{1+\tanh\left[0.3\,(x_{\rm T}-2.5)\right]\right\}x^2_{\rm T}}, \tag{17}$$

with which the additional term $-1/2$ for the stopping number is removed and Bethe's form for the stopping power is excellently reproduced. Figure 1 highlights the validity of our formula (17), where comparisons of the numeric results calculated in [35] with our parameterization (17) as well as model (16) are performed. The predictions of model (16) deviate strongly from the numeric results in the mid- and large-velocity regime. Additionally, the degeneracy effect alleviates the screening effects compared to non-degenerate plasmas.

3. Results and discussion

In this section, we present the results for the stopping power of α particles in DT plasmas as well as in DT+C mixtures. The degree of deflection describing the influence of multiple scattering effects on the energy loss of α particles is exhaustively investigated. The plasma particles are assumed to be in local thermodynamic equilibrium at the same temperature. Unless otherwise stated, the stopping powers are given in Hartree atomic units in this section.

3.1. Energy deposition and deflection in DT plasmas

The CSD stopping power ${\rm d}E/{\rm d}s$ of an α particle in a fully ionized DT plasma is displayed in figure 2, where the predictions from the BPS, original LP and modified LP models as well as from our ITM model are shown for comparison. For a weakly coupled system with BPS coupling parameter $g_{\rm BPS}\approx 0.002$ ($g^2_{\rm BPS}=\sum_c g^2_{pc}$ with $g_{pc}=\sqrt{2}z_p z_c e^2\omega_c/(4\pi\epsilon_0 k_{\rm B}T_c v_{{\rm th},c})$), we find that our calculations are in excellent agreement with the BPS results in the whole velocity region as shown in the upper panel of figure 2. In the low-energy regime, the ionic

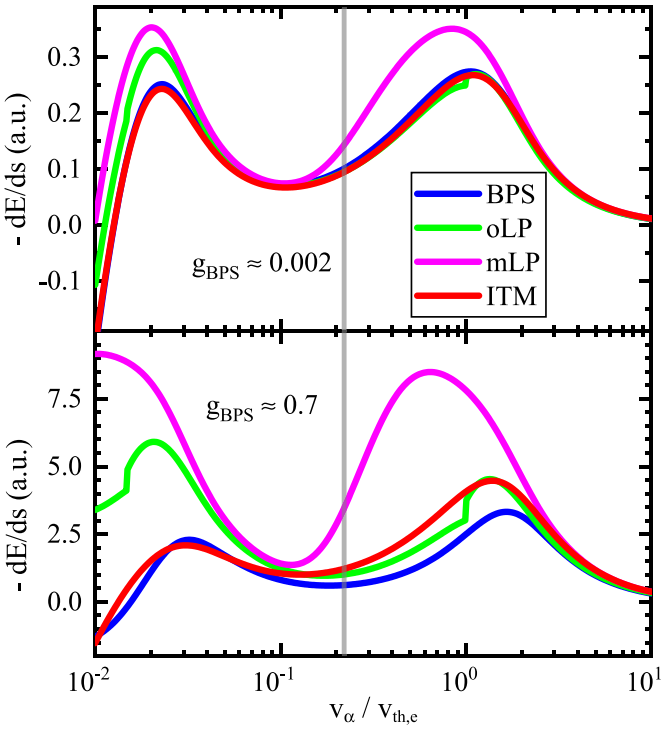

Figure 2. CSD stopping power $\mathrm{d}E/\mathrm{d}s$ of α particle in a fully ionized DT plasma with density $\rho_{DT} = 50\,\mathrm{g\,cm^{-3}}$ and electron temperatures $T_e = 10\,\mathrm{keV}$ (upper panel $g_{BPS} \approx 0.002$) and $T_e = 200\,\mathrm{eV}$ (lower panel $g_{BPS} \approx 0.7$). To compare with our predictions (ITM), results from the BPS [5], original LP ([27, 28] and LP #2 in [29]) and modified LP (LP #3 in [29]) models are also shown. The gray vertical line marks the birth energy of α particle in DT fusion (3.54 MeV).

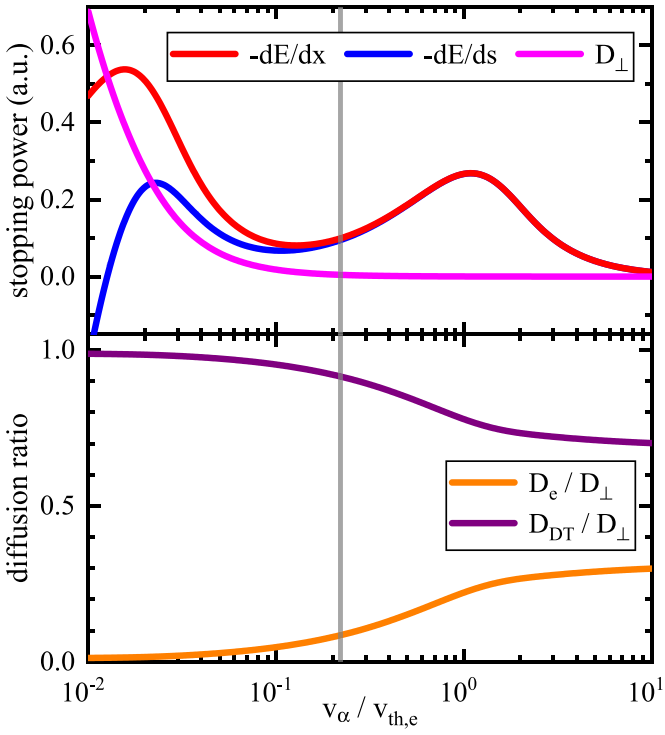

Figure 3. Upper panel: stopping powers $\mathrm{d}E/\mathrm{d}s$, $\mathrm{d}E/\mathrm{d}x$ and $\mathcal{D}_\perp$ of α particle in a fully ionized DT plasma with density $\rho_{DT} = 50\,\mathrm{g\,cm^{-3}}$ and electron temperature $T_e = 10\,\mathrm{keV}$. Lower panel: relative contribution of electrons and DT ions to the transverse diffusion. The gray vertical line marks the energy of the α particle produced in DT fusion (3.54 MeV).

stopping is dominant and displays a peak structure (Bragg peak) $v_\alpha/v_{th,e} \sim m_{DT}^{-1/2}$. The electronic stopping plays a leading role in the high-energy region and reaches the maximum near $v_\alpha/v_{th,e} \sim 1$. The electronic stopping predicted by the original LP model agrees well with the BPS and ITM models, while the ionic stopping is stronger in the original LP model than the BPS and ITM models. The modified LP model predicts larger energy losses of the α particle than all other models near the region of electronic and ionic Bragg peaks. The lower panel of figure 2 displays the CSD stopping power $\mathrm{d}E/\mathrm{d}s$ for moderately correlated plasma with $g_{BPS} \approx 0.7$. Note that the BPS model is suitable to acquire the stopping power in weakly coupled plasmas with $g_{BPS} \ll 1$. A significant difference between the different models appears in the whole velocity region. Near the electronic Bragg peak, our ITM model predicts results closer to the original LP model. Despite the visible distinction, our ITM model gives a comparable stopping power to the BPS model in the low-velocity domain near the ionic Bragg peak. Additionally, the modified LP model predicts a larger CSD stopping power than other models. This large derivation is attributed to the overestimation of collective contributions. In the modified LP model [29], the Debye length is selected as the critical parameter to separate close and distant interactions. This selection may be unsuitable, because a velocity-dependent critical impact parameter is generally required [43].

An overview of the influence of multiple scattering on the stopping power of the α particle in DT plasma is provided in figure 3. The transverse deflection caused by the multiple scattering effects is manifested by $\mathcal{D}_\perp$, i.e. the difference between the CSD and LET stopping power. From the upper panel of figure 3, it can be seen that the missing part of the multiple scattering effects in $\mathrm{d}E/\mathrm{d}s$ has a remarkable influence on the energy loss in the low-energy region, particularly near the ionic Bragg peak. This regime (left side of the gray line in figure 3) is of essential significance for understanding α-heating to DT ions. It can be also indicated from the lower panel of figure 3 that the main contribution to the transverse diffusion $\mathcal{D}_\perp$ in this regime comes from the collisions with DT ions. Regardless of the influence of the slowly changing Coulomb logarithm, the absolute contribution of plasma particle species c to the total transverse diffusion $\mathcal{D}_\perp$ is characterized by $z_c^2 m_c^{1/2}/m_T$ as revealed in equation (10). Therefore, plasma ions are expected to dominate the sideways motion of the α particle in DT plasmas.

The influence of multiple scattering on the energy deposition can be more visibly demonstrated through the degree of deflection $\langle\cos\theta\rangle$. Figure 4 illustrates the continuous change of direction of fusion-produced α particles due to scattering events as they pass through the DT fuel. The remaining energy

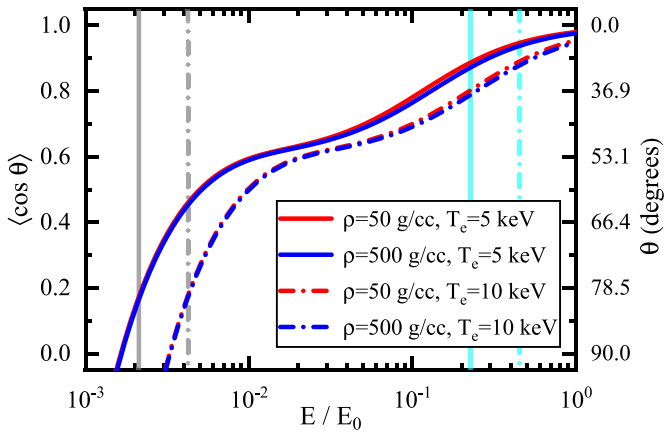

Figure 4. The degree of deflection $\langle\cos\theta\rangle$ versus the reduced residual energy of the α particle with respect to its initial energy $E_0 = 3.54\,\mathrm{MeV}$ in DT plasmas. The corresponding mean deflection angles $\theta = \arccos\langle\cos\theta\rangle$ are also shown. The residual energy is the remaining energy of the α particle after considering energy deposition into the plasma. The gray lines mark the residual energy $E = 3k_\mathrm{B}T_\mathrm{e}/2$ and the cyan lines denote the energy at which $v_\alpha = 10\,v_{\mathrm{th,DT}}$.

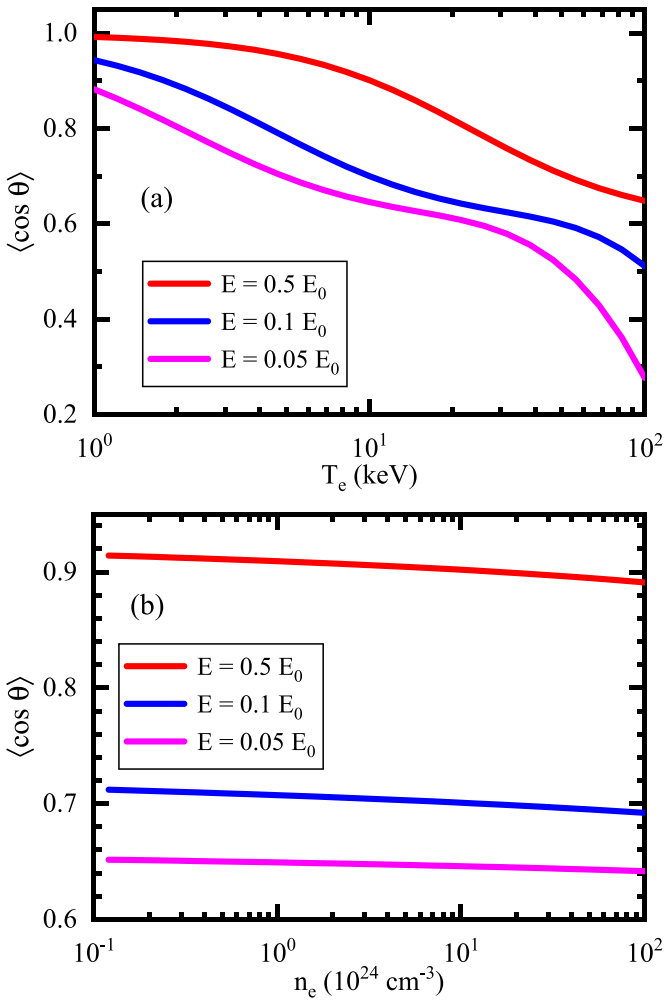

Figure 5. The degree of deflection $\langle\cos\theta\rangle$ of α particle versus temperatures (top, (*a*)) and versus densities (bottom, (*b*)) at three different energies $E/E_0 = 0.01, 0.1, 0.5$ with $E_0 = 3.54\,\mathrm{MeV}$.

of the α particle after energy has been deposited into the plasma is defined as the residual energy. When the test particle continues to deposit energy into the plasma, the lower its energy, the stronger the transverse deflection it suffers. For example, for $v_\alpha \sim 10\,v_{\mathrm{th,DT}}$ the degree of deflection is about $\theta \sim 20°$, whereas toward the end of the α range the degree of deflection is $\theta \sim 85°$. Additionally, a critical angle can be introduced, at which the incident projectile has lost the memory of its initial direction. For the deflection of energetic electrons in fast ignition for ICF, the angle $\theta_{\mathrm{cr}} = \arccos(1/\mathrm{e})$ was proposed in [14]. As depicted in figure 4, a quasi-plateau region at $\theta \sim 50°$ appears for the degree of deflection. For lower energies outside this plateau region, the deflection angle changes more quickly. Hence, the middle value of this quasi-plateau can be regarded as the critical angle.

Additionally, the degree of deflection $\langle\cos\theta\rangle$ does not change strongly with the density variation, whereas it displays a significant dependence on the temperature as shown in figure 4. Such tendencies for the temperature and density dependence are also displayed in figure 5 for three selected energies of the α particle. Increasing the temperature results in an increase in the degree of deflection, as shown in figure 4 and in the top panel of figure 5. The reason for this temperature dependence of the degree of deflection can be attributed to the fact that the velocities of plasma ions involved in the scattering are generally larger in the case of high temperatures. In this case, the energy and momentum exchange between the test particle and plasma particles is more efficient, which leads to large angle scattering and hence strong deflection from its initial direction. In the bottom panel of figure 5, we also show the change in the degree of deflection $\langle\cos\theta\rangle$ at different energies with increasing densities, where the mean deflection angle only weakly enlarges. From equations (5) and (8), it can be seen that both stopping powers have an explicit linear dependence on the density and an implicit density dependence contained in the Coulomb logarithm. As manifested in figure 6, the CSD and LET stopping powers almost linearly increase with the increase in plasma density. However, this linear dependence is eliminated because the ratio of these two stopping powers is used for the definition of the degree of deflection (2). Hence, the degree of deflection is weakly dependent on the density.

Now we apply our ITM model to analyze the experimental measurements of ion stopping around the Bragg peak [44]. The experiments were carried out at the OMEGA laser by Frenje *et al*, where the energy loss of four products, as they traversed the plasma, was measured simultaneously. In this work, the measured data from implosion 27 814 are analyzed, for which the areal density is $\rho R = 8.1\,\mathrm{mg\,cm^{-2}}$ ($\mathrm{D^3He}$ fuel areal density $\rho R = 7.1\,\mathrm{mg\,cm^{-2}}$). Using the BPS model, the best fit is obtained with the electron temperature $T_\mathrm{e} = 1.75\,\mathrm{keV}$, as reported in [44]. The upper panel of figure 7 displays the comparison among the BPS model, the experimental data and our evaluations using this temperature. Our calculations are performed using both LET (5) and CSD (8). It can be seen that

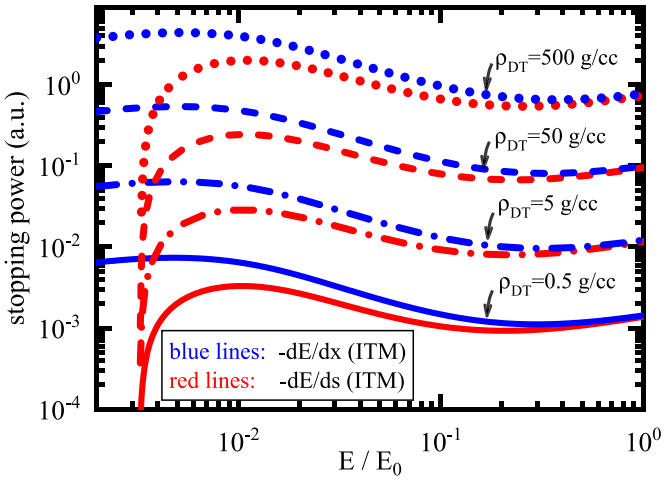

Figure 6. The CSD and LET stopping powers versus the reduced residual energy of α particle with $E_0 = 3.54\,\mathrm{MeV}$ for the temperature $T_e = 10\,\mathrm{keV}$ and different densities $\rho_{DT} = 0.5, 5, 50, 500\,\mathrm{g\,cm^{-3}}$.

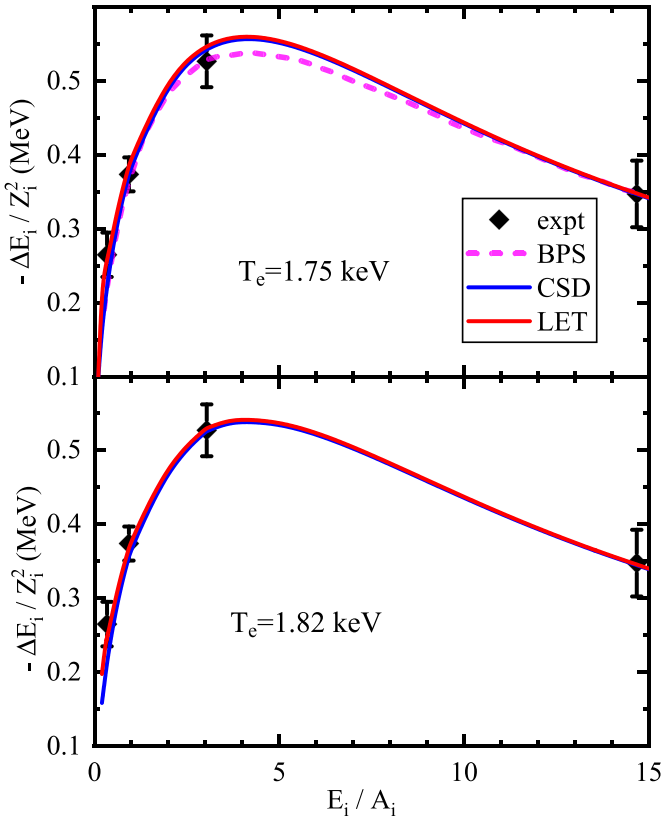

Figure 7. Measured and modeled energy loss $-\Delta E_i/Z_i^2$ with respect to E_i/A_i. The experimental and BPS results are taken from [44]. The four data (from left to right) are the energy losses for fusion products of DD-t, D^3He-α, DD-p and D^3He-p, receptively. In the modeling of the energy loss, the areal density ρR is fixed to $8.1\,\mathrm{mg\,cm^{-2}}$, while T_e is allowed to vary. The upper and lower panel denote the fits with electron temperature $T_e = 1.75\,\mathrm{keV}$ and $T_e = 1.82\,\mathrm{keV}$, respectively.

our model predicts a large energy loss for DD-p compared to the BPS model, although reasonable agreement is found with the experimental measurement. By slightly increasing the temperature to $T_e = 1.82\,\mathrm{keV}$, the experimental data can be excellently matched using the LET stopping power, as shown in the lower panel of figure 7. The CSD formalism (8) also agrees well with the experimental predictions except for the DD-t data. The values for energy loss are 0.244 MeV and 0.210 MeV using the stopping models of LET (5) and CSD (8), respectively. This difference manifests the effect of multiple scattering and transverse deflection.

3.2. Energy deposition and deflection in DT+C mixtures

As demonstrated in the previous subsection, the multiple scattering significantly affects the stopping power and the energy deposition of the α particle in DT plasmas. Uncertainty in the stopping power model is a significant source of systematic uncertainty in the inferred areal density relevant for ignition [29, 45]. In ICF systems, the DT hot spot is contaminated by other materials; for example, a 5% ablator fuel atomic mix was reported in NIF implosions [11, 12]. Because of the factor $z_c^2 m_c^{1/2}/m_T$ in the transverse diffusion (10), highly charged heavy ions can significantly influence the energy loss of α particles owing to their large masses and large related transport cross-sections. In this subsection, we will investigate the influence of C impurities on the stopping power and transverse deflection of α particles in DT plasmas.

The CSD and LET stopping powers, as well as the transverse diffusion, are illustrated in figure 8 for a DT plasma with $n_{DT} = 10^{25}\,\mathrm{cm^{-3}}$ and $T_e = 5\,\mathrm{keV}$, where the mixing ratio (ratio of concentration) of C ions to DT ions is $n_C/n_{DT} = 0.05$. Such plasma conditions are relevant for the investigation of hot spot evolution in ICF. A strong transverse diffusion of α particles in this mixture system is observed in the low-energy region, which leads to a large distinction between the CSD and LET stopping powers, as shown in the uppermost panel of figure 8. In order to acquire a deeper understanding of this large distinction between $\mathrm{d}E/\mathrm{d}s$ and $\mathrm{d}E/\mathrm{d}x$, the partial contribution from different species to the total stopping powers is studied and depicted in the middle panel of figure 8. The electronic stopping is dominant in the high-energy regime $E > 0.1\,E_0$. The most noteworthy feature is that the CSD stopping power of DT ions is much larger than that of C ions. However, if the multiple scattering effects are correctly accounted for, the LET stopping power of C ions is comparable with that induced by DT ions. The relative contributions of different species to the total transverse diffusion $\mathcal{D}_\perp$ are shown in the lowest panel of figure 8. As manifested, collisions between α particles and C ions play a leading role in the transversal motion of α particles in this case (with mixing ratio 5% and $\mathcal{D}_C/\mathcal{D}_{DT} \approx 1.7$). Collisions between α particles and plasma electrons cause a considerable transverse diffusion of the α particles, which is much smaller than that induced by ions. For another case, with a lower mixing ratio of 1% (not shown here), the transverse diffusion of α particles during energy deposition is mainly caused by the DT ions ($\mathcal{D}_C/\mathcal{D}_{DT} \approx 0.65$). Moreover, the relative contributions of the different components remain almost unchanged along with the energy deposition of the α particles. It can be concluded that the energy

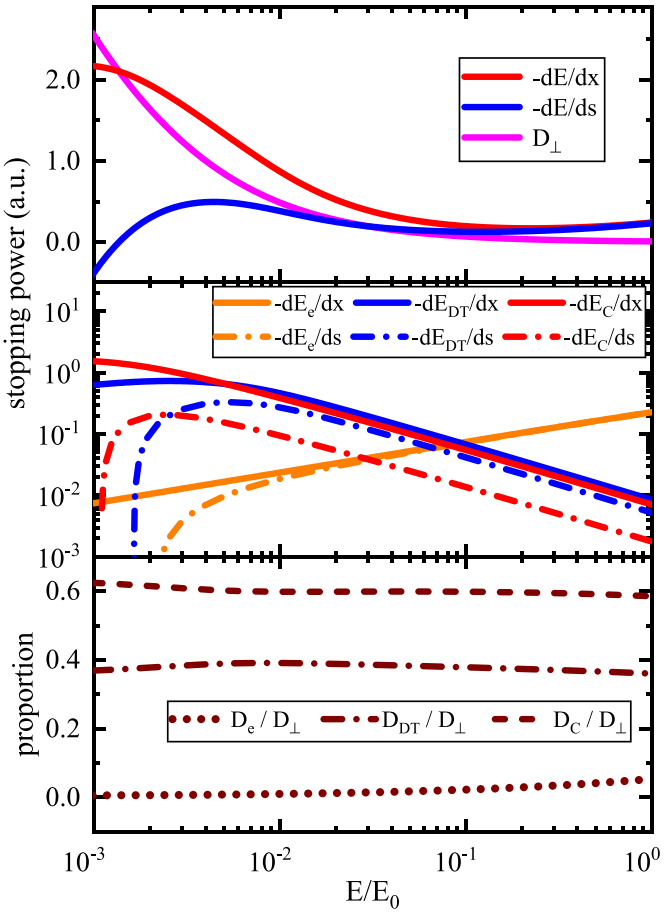

Figure 8. Upper panel: stopping powers versus the reduced residual energy of α particle with $E_0 = 3.54\,\mathrm{MeV}$ for a DT+C mixture with temperature $T_e = 5\,\mathrm{keV}$ and particle number density $n_{DT} = 10^{25}\,\mathrm{cm}^{-3}$, $n_C = 0.05\,n_{DT}$. Middle panel: partial contribution from different particle species to the corresponding total stopping powers under the same plasma condition. Lower panel: relative contribution from different particle species to the transverse diffusion $\mathcal{D}_\perp$ in the DT+C mixture.

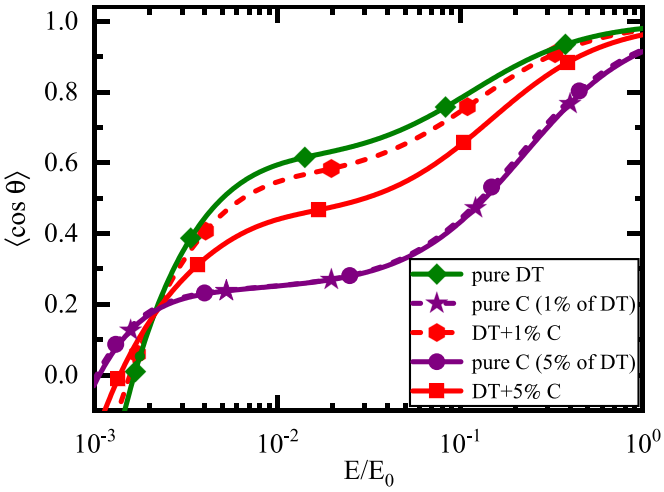

Figure 9. The degree of deflection $\langle\cos\theta\rangle$ versus the reduced residual energy of α particle with $E_0 = 3.54\,\mathrm{MeV}$ for temperature $T_e = 5\,\mathrm{keV}$ in a pure DT plasma with density $n_{DT} = 10^{25}\,\mathrm{cm}^{-3}$ (green line), in pure fully ionized C plasmas with density $n_C = x\,n_{DT}$ (purple curves) as well as in DT+C mixtures with density $n_{DT} = 10^{25}\,\mathrm{cm}^{-3}$ and $n_C = x\,n_{DT}$ (red lines). Two mixing cases with mix ratios $x = 1\%, 5\%$ are shown. Different symbols are used to mark the lines.

loss of α particles is prominently affected by the scattering between α particles and more massive ions.

Figure 9 highlights the multiple scattering effects and the related degree of deflection of α particles in pure DT and pure C plasma as well as in DT plasma mixed with C impurities. Although the number density of C ions is much smaller than the density of DT ions, the deflection of α particles in the pure C plasma is much stronger than that in the pure DT plasma, as depicted in figure 9. In particular, once an α particle with a kinetic energy of 3.54 MeV launches into the C plasma, it promptly undergoes strong collisions, which results in a relatively rapid descent of the values of $\langle\cos\theta\rangle$ in comparison with the case in the DT plasma. The degree of deflection in the DT+C mixture is located between those in the pure DT and C plasmas. As manifested in figure 9, the transverse motion of the α particle before stopping is significantly influenced by the C impurities in the intermediate energy range $0.02 \lesssim E/E_0 \lesssim 0.1$. With the increase in mixing ratio from 1% to 5%, the degree of deflection $\langle\cos\theta\rangle$ induced by the C ions is remarkably enhanced.

To investigate the dependence of the degree of deflection in DT+C mixtures on the mixing ratio, further calculations are performed for given energies of the α particle with varying concentrations of C ions. Additionally, the energy partition of the α particle to particle species c is also studied, which is defined for the CSD stopping power $\mathrm{d}E/\mathrm{d}s$ as follows [5]:

$$F_c = \int_{E_1}^{E_0} \mathrm{d}E \frac{\mathrm{d}E_c/\mathrm{d}s}{\sum_c \mathrm{d}E_c/\mathrm{d}s}. \tag{18}$$

Here, $E_1 = 3k_B T_e/2$ is taken for the numerical integration (18). For the LET stopping power $\mathrm{d}E/\mathrm{d}x$, a similar definition is applied in the calculation. It can be clearly seen from the upper panel of figure 10 that with the increase in the mixing ratio,the deflection of the α particle becomes stronger for all selected energies. In fact, such a conclusion holds for all energies smaller than the birth energy of the α particle. The lower panel of figure 10 plots the energy partition of the α particle to different plasma species with respect to the mixing ratio of C impurities. As shown in this panel, the energy of the α particle is mainly deposited on the plasma electrons under the plasma conditions considered here. The energy partition to ions predicted by the LET stopping power $\mathrm{d}E/\mathrm{d}x$ is larger than that calculated with the CSD stopping power $\mathrm{d}E/\mathrm{d}s$. With the increase in the mixing ratio, the energy partition to DT ions decreases, while the C component gains more energy from the α particles. Additionally, it seems that in the logarithmic scale the energy partition to C ions rises quasi-linearly with the increase in the mixing ratio, which corresponds to an enhancement obeying a power law in the linearity coordinates.

Finally, we investigate the energy deposition of α particle. Due to the randomizing collisions with both ions and electrons, the α particle loses energy to the hot spot and becomes

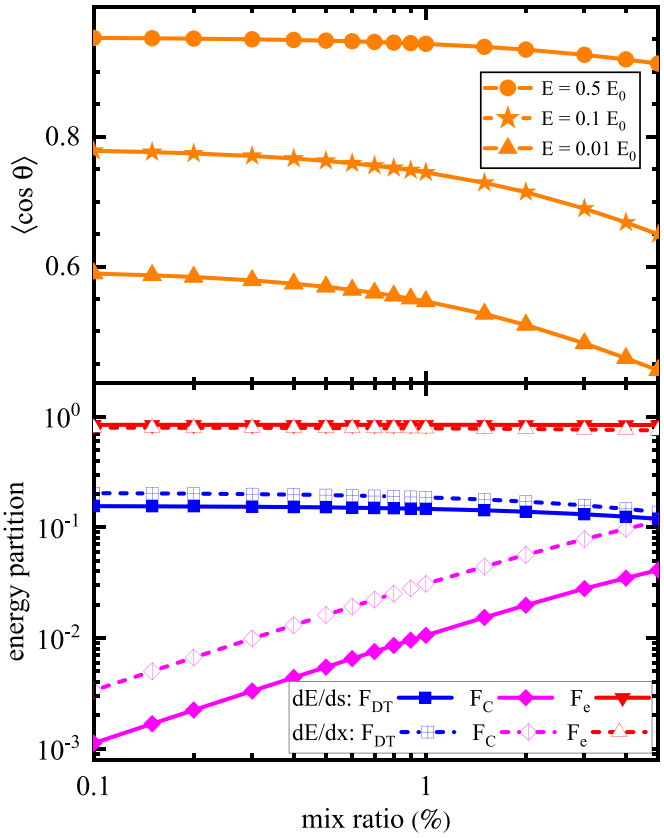

Figure 10. Upper panel: degree of deflection $\langle\cos\theta\rangle$ versus the mixing ratio with temperature $T_e = 5\,\mathrm{keV}$ and number density $n_{DT} = 10^{25}\,\mathrm{cm}^{-3}$ at three different reduced residual energies $E/E_0 = 0.01, 0.1, 0.5$. The mixing ratio is given by n_C/n_{DT}. Lower panel: the energy partition of α particle to different plasma components defined in equation (18) according to both the CSD and LET stopping powers. Lines are used to guide the eye.

thermalized at the ambient plasma temperature. These effects are characterized by the range R and the penetration depth X of the α particle, which are determined by [14]

$$R = \int_{E_0}^{E_1} \mathrm{d}E \left(\frac{\mathrm{d}E}{\mathrm{d}s}\right)^{-1}, X = \int_{E_0}^{E_1} \mathrm{d}E \left(\frac{\mathrm{d}E}{\mathrm{d}x}\right)^{-1}. \quad (19)$$

The corresponding results of range R and penetration depth X for different mixing ratios are displayed in figure 11. The results show that the range R and the penetration X become shorter and shorter with increasing mixing ratios (and also with the increasing coupling parameter g_{BPS}, whose value increases from 0.005 to 0.028). For weakly coupled plasmas, the ranges predicted by our model are in good agreement with the results of the BPS model. With the increase in coupling strength (as well as the mixing ratio), our model predicts shorter ranges than the BPS theory. Concerning the effects of transversal deflection, it is shown that the range and penetration depth of the α particle is shortened by about 21% and 27% for the case of 5% DT+C mixing according to our ITM models for CSD and LET stopping powers. Hence, more energy from the α particle is deposited into the hot spot. For further comparison, the ratio of range to penetration is depicted in figure 10

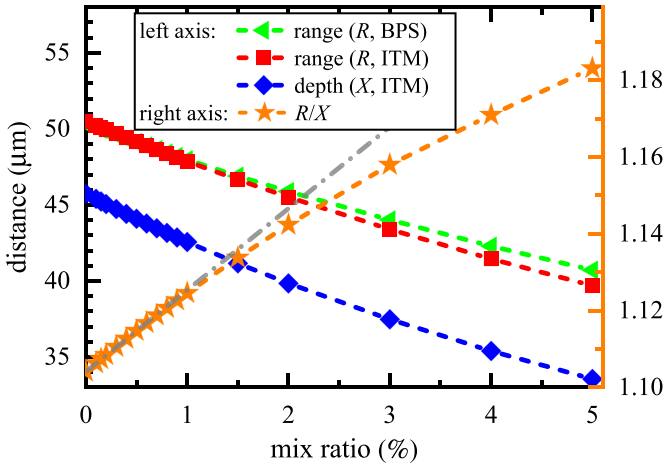

Figure 11. Left axis: the range R and penetration depth X of α particle versus the mixing ratio at fixed temperature $T_e = 5\,\mathrm{keV}$ and number density $n_{DT} = 10^{25}\,\mathrm{cm}^{-3}$. For comparison, the ranges predicted from the BPS model are also shown. Right axis: the ratio R/X, which manifests the effects of multiple scattering. The gray dashed-dotted line marks the linear increase of the range R and penetration depth X in low mixing plasmas. Dashed lines are used to guide the eye.

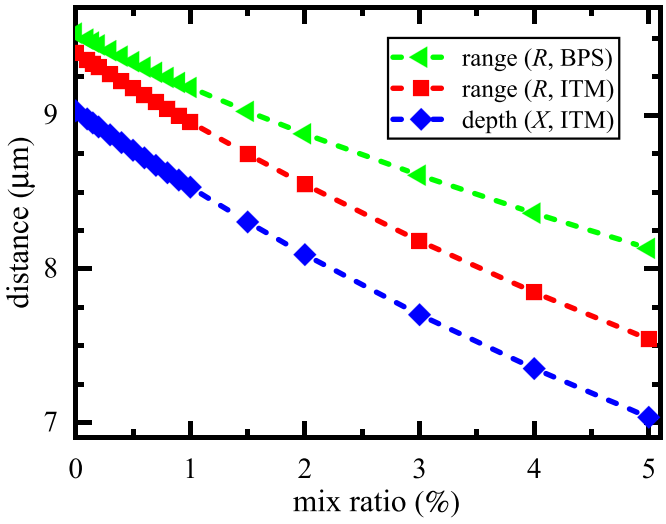

Figure 12. The same as figure 11 but for temperature $T_e = 1\,\mathrm{keV}$. Dashed lines are used to guide the eye.

(see the right axis). As the mixing concentration increases, the ratio R/X also gets larger, and a linear growth is observed for the ratio R/X in the region of low mixing concentrations. For a mixing ratio greater than 1%, the trend of growth is weaker than the linear relationship, which implies that the LET stopping power $\mathrm{d}E/\mathrm{d}x$ is more strongly affected by the impurity mixing in comparison with the CSD stopping power $\mathrm{d}E/\mathrm{d}s$.

Figure 12 displays the comparisons of the range R and the penetration depth X at a lower temperature $T_e = 1\,\mathrm{keV}$ for different mixing ratio values, where the ranges calculated from the BPS and ITM models are also compared. Under the plasma conditions presented in this figure, the BPS coupling parameter g_{BPS} increases from 0.055 for a pure DT plasma to the value of 0.32 for a DT+C mixture with mixing ratio 5%.

In comparison with the case of higher temperature shown in figure 11, the differences in the predicted ranges R become more pronounced at the same mixing ratio. For plasmas with highly charged and heavy impurities, such differences are mainly attributed to multiple scattering effects and large-angle scattering off the impurities. Therefore, it can be concluded from the comparisons shown in figures 11 and 12 that the multiple scattering effects and the resulting transverse deflection play a vital role in the investigation of energy deposition and self-heating of α particles in ICF physics.

4. Summary and conclusions

In the present investigation, we have proposed a novel approach to study the effects of multiple scattering on the stopping power and energy deposition of fusion products in ICF plasmas based on kinetic theory. Collisions between the test particles and plasma particles are described by ITM approximation with a velocity-dependent screening length. As a direct demonstration of the multiple scattering effects, the degree of deflection of test particles is defined and elaborately investigated by means of the CSD and LET stopping powers. Considering the full many-body dynamics, the effects of multiple scattering are partially included in the CSD stopping power. For the LET stopping power, multiple scattering effects are entirely taken into account within the framework of the binary collision approximation. The inherent limitations of the traditional multiple scattering theory make it difficult to apply for the calculations of the LET stopping power under plasma conditions relevant to inertial fusion. In the present study, such restrictions are bypassed by using the kinetic theory for stopping powers.

The investigation of stopping and deflection of α particles in DT plasmas and in DT plasmas mixed with C impurities manifests that the multiple scattering effects can significantly affect the energy deposition and transport of α particles in fusion plasmas. The range and the penetration depth are shortened due to the existence of C impurities and the energy deposition of an α particle increases near the end of its range. The related energy partition is also altered to a large extent. Because uncertainty in the stopping power model is an important source of systematic uncertainty in the inferred areal density, multiple scattering effects may need to be considered in modeling the energy deposition of fusion products for ignition and for critically assessing quantitative ignition requirements [3, 29, 45]. Stopping powers are also relevant to ICF diagnostics that employ charged particles including radiography and spectroscopy [4, 29]. Therefore, a deeper understanding of multiple scattering effects and the resulting transverse diffusion is of essential significance for ICF physics, which is exactly the objective of the present investigation.

In the present work, the plasma components (both ions and electrons) are assumed to be in local thermodynamic equilibrium subject to the same temperature. The velocity distribution is described by a Maxwellian distribution function. However, the distribution of the free electron velocities can deviate from the Maxwellian distribution due to the strong electrostatic field in dense plasmas [46], in particular in plasmas containing highly charged heavy impurities. Moreover, the electron degeneracy cannot be ignored if the electron temperature $T_e < 1\,\mathrm{keV}$ in the high-density regime [29, 39], so the Fermi–Dirac statistics have to be considered. Additionally, the ionic and electronic components can have different temperatures, and for such systems electron–ion temperature relaxation needs to be included for the study of stopping power [2, 47]. Furthermore, the plasma may be partially ionized, so that inelastic stopping has a remarkable contribution to the total stopping of fusion products [48]. Therefore, different inelastic processes, such as electron capture, charge transfer, as well as ionization and excitation during collisions with the target ions and electrons of the plasma, have to be taken into account for modeling the stopping powers [49, 50]. We will discuss the influence of temperature relaxation and inelastic stopping on the deflection of test particles under relevant ICF conditions in a forthcoming work.

Acknowledgments

This work was supported by the National Natural Science Foundation of China (NSFC) under Grant Nos. 12004356, 11934004 and 12274039 as well as by IAEA Research Contract No. 24243/R0.

Appendix. Derivation of expressions for the CSD and LET stopping powers

In this appendix we give a detailed derivation of the expressions of stopping powers $\mathrm{d}E/\mathrm{d}s$ and $\mathrm{d}E/\mathrm{d}x$ based on kinetic theory. The energy transfer rate of a relevant quantity is described by the collision integral as follows [2]:

$$\frac{\mathrm{d}}{\mathrm{d}t}f_{\mathrm{T}}(\mathbf{p}_{\mathrm{T}},t)=\sum_c g_c\int\frac{d^3\mathbf{p}_c}{(2\pi\hbar)^3}\int\frac{d^3\mathbf{p}_c'}{(2\pi\hbar)^3}\int\frac{d^3\mathbf{p}_{\mathrm{T}}'}{(2\pi\hbar)^3}\times\mathcal{W}(\mathbf{p}_{\mathrm{T}},\mathbf{p}_c;\mathbf{p}_{\mathrm{T}}',\mathbf{p}_c')\,\mathcal{P}(\mathbf{p}_{\mathrm{T}},\mathbf{p}_c;\mathbf{p}_{\mathrm{T}}',\mathbf{p}_c'),\quad(\mathrm{A}.1)$$

where the sum is performed over all species of plasma particles c with spin degeneracy g_c. $\mathcal{P}(\mathbf{p}_{\mathrm{T}},\mathbf{p}_c;\mathbf{p}_{\mathrm{T}}',\mathbf{p}_c')$ is the phase occupation factor for the scattering process

$$\mathcal{P}(\mathbf{p}_{\mathrm{T}},\mathbf{p}_c;\mathbf{p}_{\mathrm{T}}',\mathbf{p}_c')=f_{\mathrm{T}}(\mathbf{p}_{\mathrm{T}}')f_c(\mathbf{p}_c')\bar{f}_{\mathrm{T}}(\mathbf{p}_{\mathrm{T}})\bar{f}_c(\mathbf{p}_c)-f_{\mathrm{T}}(\mathbf{p}_{\mathrm{T}})f_c(\mathbf{p}_c)\bar{f}_{\mathrm{T}}(\mathbf{p}_{\mathrm{T}}')\bar{f}_c(\mathbf{p}_c')\quad(\mathrm{A}.2)$$

with the one-particle distribution function f and $\bar{f}=1-f$. The factor $\mathcal{W}(\mathbf{p}_{\mathrm{T}},\mathbf{p}_c;\mathbf{p}_{\mathrm{T}}',\mathbf{p}_c')$ is the transition probability for the scattering, which is directly connected to the T-matrix operator $\hat{T}$ of scattering theory

$$\mathcal{W}(\mathbf{p}_{\mathrm{T}},\mathbf{p}_c;\mathbf{p}_{\mathrm{T}}',\mathbf{p}_c')=\frac{2\pi}{\hbar}\left|\langle\mathbf{p}_{\mathrm{T}},\mathbf{p}_c|\,\hat{T}(E)\,|\mathbf{p}_{\mathrm{T}}',\mathbf{p}_c'\rangle\right|^2(2\pi\hbar)^3\times\delta(\mathbf{p}_{\mathrm{T}}+\mathbf{p}_c-\mathbf{p}_{\mathrm{T}}'-\mathbf{p}_c')\,\delta\left(\varepsilon_{\mathbf{p}_{\mathrm{T}}}+\varepsilon_{\mathbf{p}_c}-\varepsilon_{\mathbf{p}_{\mathrm{T}}'}-\varepsilon_{\mathbf{p}_c'}\right).\quad(\mathrm{A}.3)$$

It is more convenient to use the relative momentum $\mathbf{p}=(m_{\mathrm{T}}\mathbf{p}_c-m_c\mathbf{p}_{\mathrm{T}})/m_{\mathrm{T}c}$ and the total momentum $\mathbf{P}=\mathbf{p}_{\mathrm{T}}+\mathbf{p}_c$

for the scattering pair before collision. A similar variable transformation for momenta is also applied for the scattering pair after collision, and the involved quantities are marked with a prime symbol. Here, $m_{\mathrm{T}c} = m_{\mathrm{T}} + m_c$ is the total mass of the scattering pair. Inserting these variable transformations and the collision integral (A.1) in combination with the phase factor (A.2) and the transition probability (A.3) into the expression for transfer rate (3) yields

$$\frac{\mathrm{d}}{\mathrm{d}t}\langle\mathcal{A}\rangle = \frac{2\pi}{\hbar n_{\mathrm{T}}}\sum_c g_c \int \frac{d^3\mathbf{p}}{(2\pi\hbar)^3}\int \frac{d^3\mathbf{P}}{(2\pi\hbar)^3}\int \frac{d^3\mathbf{p}'}{(2\pi\hbar)^3} \times T^2_{\mathrm{T}c}(\mathbf{p},\mathbf{p}')\,\delta\left(\frac{\mathbf{p}^2}{2\mu_{\mathrm{T}c}} - \frac{\mathbf{p}'^2}{2\mu_{\mathrm{T}c}}\right)\left\{\mathcal{A}(\mathbf{p}'_{\mathrm{T}}) - \mathcal{A}(\mathbf{p}_{\mathrm{T}})\right\} \times f_{\mathrm{T}}(\mathbf{p}_{\mathrm{T}})\, f_c(\mathbf{p}_c)\,[1 - f_c(\mathbf{p}'_c)]\,, \tag{A.4}$$

where the momenta $\mathbf{p}_{\mathrm{T}}, \mathbf{p}'_{\mathrm{T}}, \mathbf{p}_c, \mathbf{p}'_c$ are determined via the inverse transformation of the relative and total momenta $\mathbf{p}, \mathbf{p}', \mathbf{P}, \mathbf{P}'$. For the derivation of transfer rate (A.4), the on-shell T-matrix is applied, which is connected to the quantum differential cross-section [2]

$$T^2_{\mathrm{T}c}(\mathbf{p},\mathbf{p}') = \frac{(2\pi)^2\hbar^4}{\mu^2_{\mathrm{T}c}}\frac{\mathrm{d}\sigma_{\mathrm{T}c}}{\mathrm{d}\Omega_{\mathbf{pp}'}}\,. \tag{A.5}$$

To simplify the problem, the test particle is assumed to be sharply distributed around its momentum, which is described by a Dirac delta distribution $f_{\mathrm{T}}(\mathbf{p}_{\mathrm{T}}) = (2\pi\hbar)^3 n_{\mathrm{T}}\delta(\mathbf{p}_{\mathrm{T}} - m_{\mathrm{T}}\mathbf{v}_{\mathrm{T}})$. Each species c in the plasma system is assumed to be in the local thermodynamic equilibrium subject to the same temperature. In this work, the Maxwell–Boltzmann distribution is used for the function f_c and $1 - f_c$ is slightly different from 1 for all momenta. The electron degeneracy can be significant for relative low-temperature and high-density plasmas [29, 39, 51, 52]. In moderate degenerate plasmas, these effects can be approximately taken into account by using an effective temperature, with which the Fermi–Dirac distribution function can be approximated by Maxwellian distribution [39]. However, in strong degenerate plasmas, the Fermi–Dirac distribution has to be taken into account, and also the term $1 - f_c$ cannot be approximated by the constant 1 any more. The physical systems relevant to ICF are hot dense plasmas with temperature $T_{\mathrm{e}} \gtrsim 1\,\mathrm{keV}$. Hence, the Maxwell–Boltzmann distribution function is a reasonable and sufficient approximation for the particle distribution f_c. With these assumptions, we obtain the following expression for the transfer rate of $\mathcal{A}(\mathbf{p}_{\mathrm{T}})$

$$\frac{\mathrm{d}}{\mathrm{d}t}\langle\mathcal{A}\rangle = \frac{2}{\mu_{\mathrm{T}c} n_{\mathrm{T}}}\sum_c g_c \int \frac{d^3\mathbf{p}}{(2\pi\hbar)^3}\int \frac{d^3\mathbf{P}}{(2\pi\hbar)^3}\int d^3\mathbf{p}'\,\frac{\mathrm{d}\sigma_{\mathrm{T}c}}{\mathrm{d}\Omega_{\mathbf{pp}'}} \times \delta\left(\mathbf{p}^2 - \mathbf{p}'^2\right)\left\{\mathcal{A}(\mathbf{p}'_{\mathrm{T}}) - \mathcal{A}(\mathbf{p}_{\mathrm{T}})\right\} f_{\mathrm{T}}(\mathbf{p}_{\mathrm{T}}) f_c^{\mathrm{MB}}(\mathbf{p}_c)\,. \tag{A.6}$$

In order to achieve expressions for the CSD and LET stopping powers that are available for numeric computation, the quantity $\mathcal{A}(\mathbf{p}_{\mathrm{T}})$ has to be specified. Using $\mathcal{A}_{\mathrm{M}}(\mathbf{p}'_{\mathrm{T}}) - \mathcal{A}_{\mathrm{M}}(\mathbf{p}_{\mathrm{T}}) = \mathbf{v}_{\mathrm{T}} \cdot (\mathbf{p}'_{\mathrm{T}} - \mathbf{p}_{\mathrm{T}})$ for the LET stopping power dE/dx [2, 22], we obtain the following representation for the LET stopping power:

$$\frac{\mathrm{d}E}{\mathrm{d}x} = \sum_c \int_0^\infty \mathrm{d}p\, p^2\, \mathcal{Q}_{\mathrm{T}c}(p)\, \mathcal{G}_{\mathrm{T}c}(v_{\mathrm{T}}, p)\, \mathcal{F}_{\mathrm{M}}(w) \tag{A.7}$$

with the function $\mathcal{F}_{\mathrm{M}}(w) = \sinh(w) - w\cosh(w)$ and $w = 2v_{\mathrm{T}}p/(\mu_{\mathrm{T}c} v^2_{\mathrm{th},c})$. The transport cross-section $\mathcal{Q}_{\mathrm{T}c}(p)$ is determined from the quantum differential cross-section as

$$\mathcal{Q}_{\mathrm{T}c}(p) = \int \mathrm{d}\Omega_{\mathbf{pp}'}\,(1 - \cos\theta_{\mathbf{pp}'})\frac{\mathrm{d}\sigma_{\mathrm{T}c}}{\mathrm{d}\Omega_{\mathbf{pp}'}}, \tag{A.8}$$

which is also known as the momentum transfer cross-section. The function $\mathcal{G}_{\mathrm{T}c}(v_{\mathrm{T}}, p)$ is defined as

$$\mathcal{G}_{\mathrm{T}c}(v_{\mathrm{T}}, p) = \frac{n_c\, v_{\mathrm{th},c}}{\sqrt{\pi} v^2_{\mathrm{T}} \mu^2_{\mathrm{T}c}} \exp\left[-\frac{v^2_{\mathrm{T}}}{v^2_{\mathrm{th},c}} - \frac{p^2}{\mu^2_{\mathrm{T}c} v^2_{\mathrm{th},c}}\right]. \tag{A.9}$$

Similarly, the resulting formula for the CSD stopping power is

$$\frac{\mathrm{d}E}{\mathrm{d}s} = \sum_c \int_0^\infty \mathrm{d}p\, p^2\, \mathcal{Q}_{\mathrm{T}c}(p)\, \mathcal{G}_{\mathrm{T}c}(v_{\mathrm{T}}, p)\, \mathcal{F}_{\mathrm{E}}(w) \tag{A.10}$$

with $\mathcal{F}_{\mathrm{E}}(w) = [1 + p\,w/(m_{\mathrm{T}} v_{\mathrm{T}})]\sinh(w) - w\cosh(w)$. The transverse diffusion $\mathcal{D}_\perp$ takes the following form:

$$\mathcal{D}_\perp = \sum_c \int_0^\infty \mathrm{d}p\, p^2\, \mathcal{Q}_{\mathrm{T}c}(p)\, \mathcal{G}_{\mathrm{T}c}(v_{\mathrm{T}}, p)\, \mathcal{F}_\perp(w) \tag{A.11}$$

with $\mathcal{F}_\perp(w) = pw\sinh(w)/(m_{\mathrm{T}} v_{\mathrm{T}})$. Using the velocity-dependent Coulomb logarithm (7) to replace the transport cross-section $\mathcal{Q}_{\mathrm{T}c}(p)$ and introducing other reduced variables, the expressions (5), (8) and (10) are achieved.

ORCID iDs

Chengliang Lin https://orcid.org/0000-0001-8993-1220
Bin He https://orcid.org/0000-0003-2635-3456

References

[1] Ziegler J.F., Biersack J. and Littmark U. 1985 *The Stopping and Range of Ions in Solids* (London: Pergamon)
[2] Kremp D., Schlanges M. and Kraeft W.D. 2005 *Quantum Statistics of Nonideal Plasmas* (Berlin: Springer)
[3] Atzeni S. and Meyer-Ter-Vehn J. 2004 *The Physics of Inertial Fusion: Beam Plasma InterAction, Hydrodynamics, Hot Dense Matter* (New York: Oxford University Press)
[4] Zylstra A.B. and Hurricane O.A. 2019 *Phys. Plasmas* **26** 062701
[5] Brown L.S., Preston D.L. and Singleton R.L. Jr 2005 *Phys. Rep.* **410** 237
[6] Krokhin O.N. and Rozanov V.B. 1973 *Sov. J. Quantum Electron.* **2** 393
[7] Molvig K., Schmitt M.J., Albright B.J., Dodd E.S., Hoffman N.M., McCall G.H. and Ramsey S.D. 2016 *Phys. Rev. Lett.* **116** 255003
[8] Montgomery D.S. *et al* 2018 *Phys. Plasmas* **25** 092706

[9] Landen O.L. *et al* 2010 *Phys. Plasmas* **17** 056301
[10] Fu Z.-G., Wang Z., Mo C., Li D., Li W., Lu Y., Kang W., He X.-T. and Zhang P. 2020 *Phys. Rev.* E **101** 053209
[11] Regan S.P. *et al* 2013 *Phys. Rev. Lett.* **111** 045001
[12] Ma T. *et al* 2013 *Phys. Rev. Lett.* **111** 085004
[13] Zylstra A.B. *et al* 2020 *Phys. Plasmas* **27** 092709
[14] Li C.K. and Petrasso R.D. 2004 *Phys. Rev.* E **70** 067401
[15] Atzeni S., Schiavi1 A. and Davies J.R. 2009 *Plasma Phys. Control. Fusion* **51** 015016
[16] Bethe H.A., Rose M.E. and Smith L.P. 1938 *Proc. Amer. Phil. Soc.* **78** 573 (available at: www.jstor.org/stable/984803)
[17] Lewis H.W. 1950 *Phys. Rev.* **78** 526
[18] Mahdavi M. and Koohrokhi T. 2012 *Phys. Rev.* E **85** 016405
[19] Li C.K. and Petrasso R.D. 1995 *Phys. Plasmas* **2** 2460
[20] Gericke D.O., Schlanges M. and Kraeft W. 1996 *Phys. Lett.* A **222** 241
[21] Gericke D.O. and Schlanges M. 1998 *Phys. Rev.* E **60** 904
[22] Zwicknagel G., Toeppfer C. and Reinhard P.G. 1999 *Phys. Rep.* **309** 117
[23] Sivukhin D.V. 1966 Coulomb collosions in a fully ionized plasma *Reviews of Plasma Physics* vol 4, ed M.A. Leontovich (New York: Consultants Bureau)
[24] Morawetz K. and Röpke G. 1996 *Phys. Rev.* E **54** 4134
[25] Atzeni S., Schiavi A., Califano F., Cattani F., Cornolti F., Del Sarto D., Liseykina T.V., Macchi A. and Pegoraro F. 2005 *Comput. Phys. Commun.* **169** 153
[26] Atzeni S., Schiavi A., Honrubia J.J., Ribeyre X., Schurtz G., Nicolaï P., Olazabal-Loumé M., Bellei C., Evans R.G. and Davies J.R. 2008 *Phys. Plasmas* **15** 056311
[27] Li C. and Petrasso R. 1993 *Phys. Rev. Lett.* **70** 3059
[28] Li C.K. and Petrasso R.D. 2015 *Phys. Rev. Lett.* **114** 199901
[29] Zylstra A.B., Rinderknecht H.G., Frenje J.A., Li C.K. and Petrasso R.D. 2019 *Phys. Plasmas* **26** 122703
[30] Ding Y.H., White A.J., Hu S.X., Certik O. and Collins L.A. 2018 *Phys. Rev. Lett.* **121** 145001
[31] White A.J., Collins L.A., Nichols K. and Hu S. 2022 *J. Phys.: Condens. Matter* **34** 174001
[32] Ferrariis L. and Arista N.R. 1984 *Phys. Rev.* A **29** 2145
[33] Bernstein D.J., Baalrud S.D. and Daligault J. 2019 *Phys. Plasmas* **26** 082705
[34] Gould H.A. and DeWitt H.E. 1967 *Phys. Rev.* **155** 68
[35] Zwicknagel G. 2002 *Nucl. Instrum. Methods Phys. Res.* B **197** 22
[36] Joachain C.J. 1975 *Quantum Collision Theory* (Belgium: Universite Libre de Bruxelles)
[37] Lin C., He B., Wu Y. and Wang J. 2023 *Plasma Phys. Control. Fusion* **65** 055005
[38] Landau L.D. and Lifshitz E.M. 1960 *Mechanics* (Oxford: Pergamon)
[39] Clauser C.F. and Arista N.R. 2018 *Phys. Rev.* E **97** 023202
[40] Gericke D.O. and Schlanges M. 2003 *Phys. Rev.* E **67** 037401
[41] Cayzac W. *et al* 2017 *Nat. Commun.* **8** 15693
[42] Arista N.R. and Sigmund P. 2007 *Phys. Rev.* A **76** 062902
[43] Sigmund P. 1996 *Phys. Rev.* A **54** 3113
[44] Frenje J.A., Grabowski P.E., Li C.K., Séguin F.H., Zylstra A.B., Gatu Johnson M., Petrasso R.D., Glebov V.Y. and Sangster T.C. 2015 *Phys. Rev. Lett.* **115** 205001
[45] Zylstra A.B. *et al* 2014 *Phys. Plasmas* **21** 112701
[46] He B. and Wang J.G. 2013 *Nucl. Fusion* **53** 093009
[47] He B., Wang Z.G. and Wang J.G. 2018 *Phys. Plasmas* **25** 012704
[48] He B., Liu C.L., Liu L. and Wang J.G. 2015 *Nucl. Fusion* **55** 063039
[49] Peter T. and Meyer-Ter-Vehn J. 1991 *Phys. Rev.* A **43** 2015
[50] Frank A. *et al* 2013 *Phys. Rev. Lett.* **110** 115001
[51] Dharma-wardana M.W.C. and Perrot F. 2000 *Phys. Rev. Lett.* **84** 959
[52] Hayes A.C. *et al* 2020 *Nat. Phys.* **16** 432